An MRI-Based Method to Align the Compressive Loading Axis for Human Cadaveric Knees

K. J. Martin
Biomedical Engineering Program,
University of California,
One Shields Avenue,
Davis, CA 95616

C. P. Neu
Department of Orthopedics,
University of California at Davis Medical Center,
2315 Stockton Boulevard,
Sacramento, CA 95817

M. L. Hull[1]
Department of Mechanical Engineering,
and Biomedical Engineering Program,
University of California,
One Shields Avenue,
Davis, CA 95616
e-mail: mlhull@ucdavis.edu

There is a need to align the mechanical axis of the tibia with the axis of loading for studies involving tibiofemoral compression to interpret results and to ensure repeatability of loading within and among specimens. Therefore, the objectives of this study were (1) to develop a magnetic resonance imaging (MRI)-based alignment method for use with apparatuses applying tibiofemoral joint compression, (2) to demonstrate the usefulness of the method by aligning cadaveric knees in an apparatus that could apply tibiofemoral joint compression, and (3) to quantify the error associated with the alignment method. A four degree-of-freedom adjustable device was constructed to allow determination and alignment of the mechanical axis of the tibia of cadaveric knee joints with the axis of loading of an apparatus applying tibiofemoral joint compression. MRI was used to determine the locations of bony landmarks in three dimensions defining the mechanical axis of the tibia relative to an initial orientation of the four degree-of-freedom device. Adjustment values of the device were then computed and applied to the device to align the mechanical axis of the tibia with the axis of a compressive loading apparatus. To demonstrate the usefulness of the method, four cadaveric knees were aligned in the compressive loading apparatus. The vectors describing the mechanical axis of the tibia and the loading axis of the apparatus before and after adjustment of the four degree-of-freedom device were computed for each cadaveric knee. After adjustment of the four degree-of-freedom device, the mechanical axis of the tibia was collinear with the loading axis of the apparatus for each cadaveric knee. The errors in the adjustment values introduced by inaccuracies in the MR images were quantified using the Monte Carlo technique. The precisions in the translational and rotational adjustments were 1.20 mm *and* 0.90 deg *respectively. The MR-based alignment method will allow consistent interpretation of results obtained during tibiofemoral compressive studies conducted using the apparatus described in this paper by providing a well-defined loading axis. The alignment method can also be adapted for use with other apparatuses applying tibiofemoral compression.* [DOI: 10.1115/1.2800765]

Keywords: knee, compression, MRI, alignment, apparatus, rotation, translation

Introduction

Experimental studies of the tibiofemoral joint subjected to compressive loading are commonly performed to study tibiofemoral contact [1–4]. Tibiofemoral alignment has also been shown to affect contact pressures and areas during compression of the knee joint [5] and knee joint arthroplasties [6]. Hence, to interpret results obtained using tibiofemoral compression, to ensure repeatability of assigned loading within and among specimens, and to provide reproducibility between studies, there is a need to achieve loading of the tibiofemoral joint along a specified axis.

Notwithstanding the need to achieve loading along a specified axis in studies of tibiofemoral contact, there is little consistency in the methods that have been used to establish alignment of the compressive loading axis, and the methods have limitations. In some studies [1,3,4], little to no description of knee joint alignment with the loading axis of the material testing system used was provided. Biplanar radiographs have been used to determine anatomical landmark locations in the knee to define coordinate systems and loading axes [7]. This method, however, requires additional equipment, such as an alignment jig and analogous bone-holding components on the knee loading apparatus. External palpation has also been used for an appropriate placement of bone-holding clamps [8]; however, this method is subjective and may not be highly repeatable or reproducible. Alternatively, a knee loading apparatus may be equipped to establish a functional axis alignment by which axes are determined by minimizing coupled motions of the knee during the prescribed motion [9]. Components required to determine functional axes, including sensors and fixtures allowing adjustability in six degrees of freedom for both the tibia and femur, result in a complex loading apparatus. The corresponding trial and error alignment method can additionally be time consuming.

Magnetic resonance imaging (MRI) may be used to spatially locate bony landmarks in three dimensions. These locations can then be used to establish and maintain a specified axis of loading for a particular knee specimen. Given the need to load along a specified axis for tibiofemoral compression studies and the advantages of MRI to locate this axis, the objectives of this study were (1) to develop an MRI-based alignment method for use with apparatuses applying tibiofemoral joint compression, (2) to demonstrate the usefulness of the method by aligning cadaveric knees in an apparatus that could apply tibiofemoral joint compression, and (3) to quantify the error associated with our alignment method.

Methods and Materials

Alignment Method. Anatomically based coordinate systems were first established for the tibiofemoral joint (Fig. 1). For the

[1]Corresponding author.

Contributed by the Bioengineering Division for publication in the JOURNAL OF BIOMECHANICAL ENGINEERING. Manuscript received June 1, 2006; final manuscript received April 30, 2007. Review conducted by Noshir Langrana.

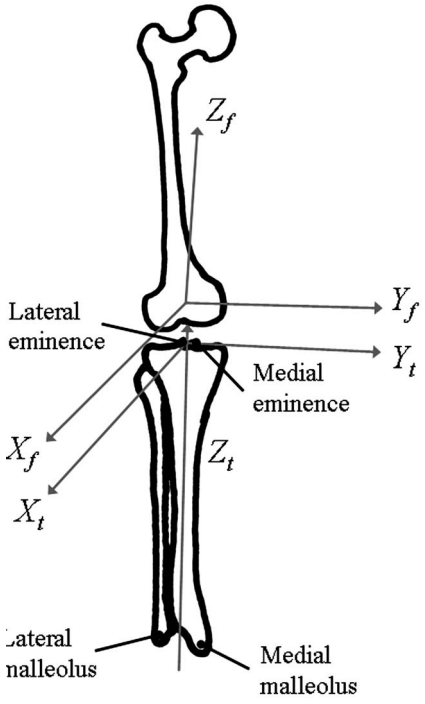

Fig. 1 Local coordinate systems for tibia and femur. See text for the definition of coordinate systems.

tibial coordinate system, the origin was defined as the point located midway between the tips of tibial eminences. The Z_t axis, often called the mechanical axis of the tibia [10], was defined as a line passing through a point midway between the lateral and medial maleoli and the origin of the tibial coordinate system ($+Z_t$ proximal). The X_t axis was defined as the cross product of Z_t and a line connecting the tips of the tibial eminences ($+X_t$ anterior). The Y_t axis was then defined as the cross product of Z_t and X_t ($+Y_t$ medial for a right knee). For the femoral coordinate system, only a flexion-extension axis was required for later positioning of the knee. Therefore, the Y_f axis was defined as a line passing through the centers of circles estimated from the posterior portions of the femoral condyles ($+Y_f$ medial for a right knee), which is also known as the cylindrical axis of the knee [11]. For the sake of completing the femoral coordinate system, the origin was defined as the midpoint between the most medial and lateral aspects of the medial and lateral condyles, respectively, which intersected Y_f. The X_f axis was defined as the cross product of Y_f and a line from the origin of the femoral coordinate system to the center of the femoral head ($+X_f$ anterior), and the Z_f axis was defined as the cross product of X_f and Y_f ($+Z_f$ proximal).

Once defined, the tibial mechanical axis was located for each of four cadaveric knees in three dimensions and aligned with the compressive loading axis of an apparatus using a four degree-of-freedom (4-DOF) adjustable attachment device (Fig. 2). The knees from four whole human cadaveric legs (all male, average age: 47.8 years, range: 36–55 years) free from degenerative joint disease or defects, as determined by visual inspection and viewing anterior-posterior (A-P) and lateral radiographs, were first prepared by dissecting soft tissues from the tibia and femur at a

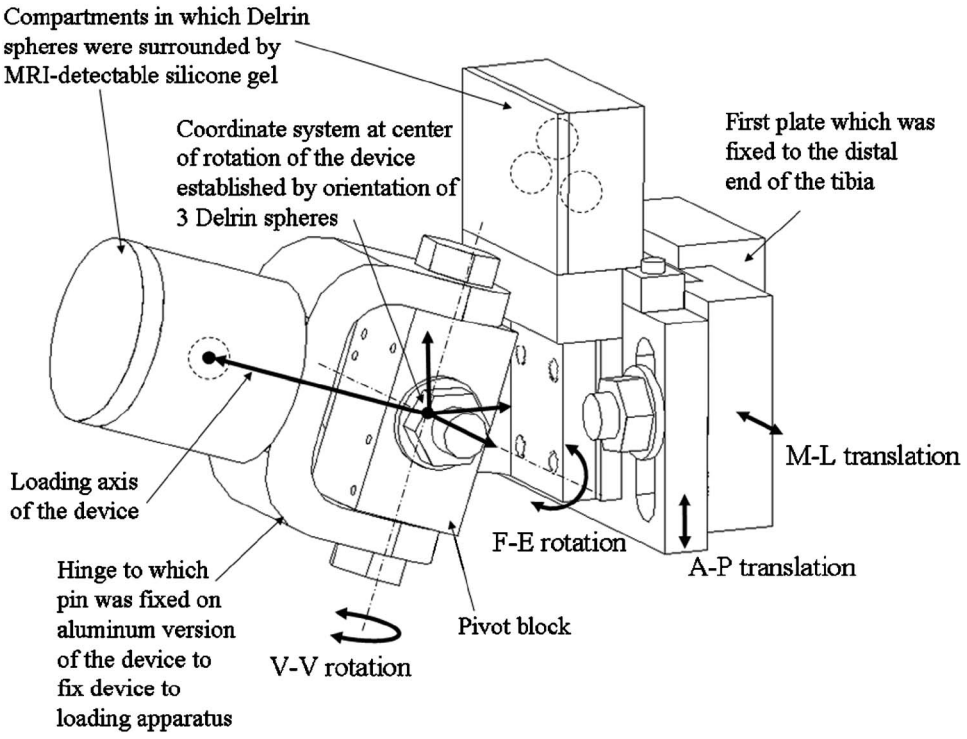

Fig. 2 Diagram of the plastic version of the 4-DOF adjustable attachment device with components in non-neutral positions. The aluminum version of the device had the same dimensions, but did not have compartments encasing Delrin spheres surrounded by silicone gel. Instead the aluminum version had a pin fixed to the end of the hinge, which was used to fix the device and, thus, the specimen to a loading apparatus. The pin on the aluminum device was collinear with the vector on the analogous plastic device from the center of rotation to the single sphere at its end shown here. M-L and A-P translations of each device were achieved by sliding slotted plates relative to the first plate, which was attached to the distal end of the tibia. F-E and V-V rotations were achieved by revolving the hinge and pivot block respectively about the two axes of the universal joint.

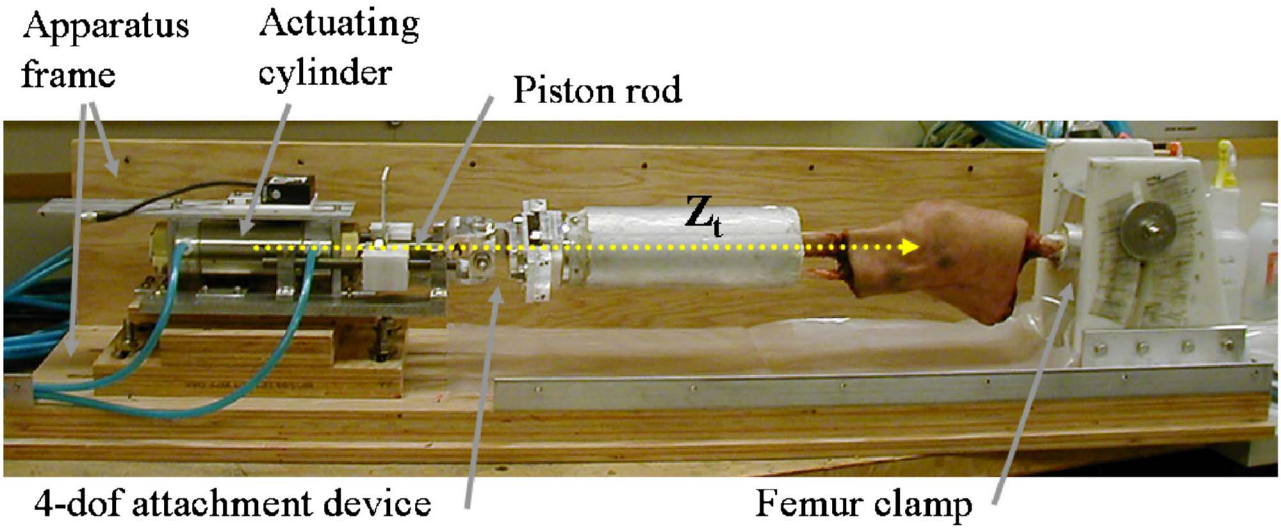

Fig. 3 Specimen aligned in an apparatus (top and front parts of the frame are removed) that can apply tibiofemoral compression such that the mechanical axis of the tibia coincides with the axis of loading. The specimen is flexed 10 deg from its 0 deg reference position.

distance of approximately 13 cm in either direction from the joint line. For each specimen, the foot was removed while maintaining a relative alignment of the lateral and medial maleoli by preserving connective tissues between distal ends of the tibia and fibula. The tibia was potted in an acrylic tube having a plastic end cap using polymethyl methacrylate (PMMA) by fixing the femur horizontally and allowing the tibia to hang free, with its mechanical axis aligned approximately with the long axis of a vertically oriented acrylic tube. The tube and specimen were left undisturbed for at least 30 min so that the PMMA could fully cure. The plastic 4-DOF device was attached to the end cap on the distal end of the tube. To determine the 3D orientation of each tibia relative to the 4-DOF device, a group of three Delrin spheres (each with a diameter of 12.7 mm±0.025 mm) surrounded by an MRI-detectable silicone gel (Sylgard 527 dielectric gel, Dow Corning Corporation, Midland, MI) in a rectangular compartment was located on the 4-DOF device on the plate used for A-P adjustment at a known translation from the center of rotation of the device when each component of the device was in its neutral position. A single Delrin sphere, surrounded by silicone gel in a cylindrical compartment, was located at the distal end of the device at a known distance from the center of rotation of the device.

Next, MR images were collected to determine adjustment values required to align the loading axis of the 4-DOF device with the mechanical axis of each tibia. A 1.5 T MRI scanner (GE Medical Systems, Waukesha, WI) was used to collect a set of images of the device and distal end of the tibia as well as a set of images of the knee. Device and distal tibia images were obtained using spoiled gradient echo sequence (SPGR) (TR=200, TE =1.532, flip angle=80, slice thickness=5, spacing between slices=0.5 mm, number of averages=4, resolution=1.48 $\times$1.48 mm^2, and field of view=380$\times$380 cm^2), and knee images were obtained using a 3D gradient recalled echo sequence (GRE) (TR=20.6, TE=9.625, flip angle=20, slice thickness=1.5, spacing between slices=0, number of averages=1, resolution=0.47 $\times$0.47 mm^2, and field of view=240$\times$240 cm^2). Bony landmarks and the centers of the Delrin spheres on the 4-DOF device were then located in three dimensions using MR images, and 3D locations were used to determine adjustment values for the 4-DOF device as detailed in the Appendix.

Once adjustment values were determined (details in the Appendix), the plastic 4-DOF device was replaced with an aluminum version of the device, which was aligned with the mechanical axis of the tibia. The plastic 4-DOF device was first removed, and an aluminum end cap, which had the same holes as the plastic end cap to define the location of the device, was bolted and cemented to the acrylic tube in place of the plastic end cap. The acrylic tube was then potted in an aluminum tube using PMMA to increase the rigidity of the tibial end of the specimen. Using known adjustment values, rotations of the hinge parts of the device about the pivot block were first achieved to the closest 0.5 deg increment. These rotations were measured by placing each hinge in a custom fixture, attaching a small extension piece to the pivot block, aligning the center of the extension piece to the desired 0.5 deg increment scribed onto the fixture, and tightening bolts through each hinge. The first plate of the 4-DOF device was bolted to the aluminum end cap, and medial-lateral (M-L) and A-P translations of the 4-DOF device were achieved to the nearest millimeter while attaching the slotted plates, to which the universal joint (composed of the hinge components and the pivot block) was attached, to the first plate of the device. A pin with an orthogonal through-hole projected from the most distal hinge part in lieu of the cylindrical compartment located on the plastic version of the device, which could be slipped into a mating part on the end of the piston rod of the actuating cylinder of the loading apparatus to fix the alignment of the loading axis with Z_t.

A reference position was then defined for each specimen. First, the flexion-extension or cylindrical axis [11] of the knee was located by flexing and extending the knee and locating a medial and lateral point on the knee, which did not move during the flexion-extension motion [12]. This axis was marked on the skin of the knee. The femoral head and greater trochanter were next removed from the femur, and the remaining femoral bone was potted in an aluminum tube using PMMA. The femoral bone tube was inserted into the femur clamp on the loading apparatus, and the 4-DOF device was fixed to the actuating piston rod (Fig. 3). The loading apparatus allowed adjustment of the knee specimen in six degrees of freedom, and the specimen was moved such that the flexion-extension (F-E) axis marked on the specimen was aligned with the F-E axis of the apparatus. A-P, M-L, and compression-distraction (C-D) translations, in addition to varus-valgus (V-V) and internal-external (I-E) rotations, were achieved by moving the slotted plate on which the actuating cylinder was attached relative to the frame of the apparatus, while the F-E rotation, additional I-E rotation, and additional C-D translation were achieved with the femur clamp. After locking the tibial side of the specimen in place and locking the I-E rotation and C-D translation in place on the femoral side, the specimen was manually extended on the femoral side

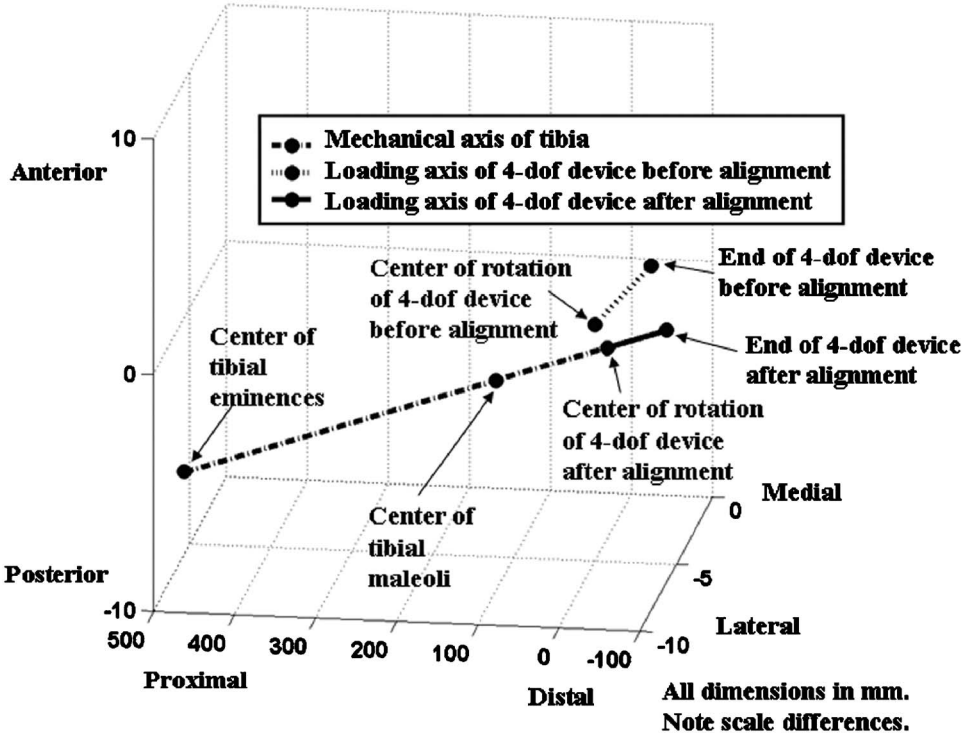

Fig. 4 Orientation of the loading axis of the 4-DOF device with the tibial mechanical axis of Specimen 2 before and after alignment of the device. After alignment, the mechanical axis was collinear with the loading axis.

until resistance was felt [13,14]. The specimen was then defined to be in a 0 deg flexion reference position from which alternative flexion or hyperextension angles could be achieved.

The alignment method with its attendant equations described in the Appendix was verified. For each knee, vectors describing the mechanical axis of the tibia and the initial loading axis of the apparatus were computed and plotted. Computed A-P, M-L, I-E, and V-V adjustment values were then used to determine and plot the new loading axis of the apparatus. Alignment was deemed successful if the mechanical axis of the tibia was collinear with the new loading axis.

Error Analysis. To quantify the error associated with the alignment method, the precisions of the adjustments computed by the algorithm described in the Appendix were determined using the Monte Carlo technique. The Monte Carlo technique was used twice, once to determine the variance of the normally distributed error, which should be applied to the coordinate inputs as a result of inaccuracies in the MR imaging, and a second time to determine the precision in the adjustments knowing the error in coordinate inputs.

To determine the error in the coordinate inputs, the distance between the centers of each pair of the four Delrin spheres of the 4-DOF device (e.g., $|\mathbf{r}_g^{p1/g0} - \mathbf{r}_g^{p2/g0}|$) was determined from the MR images. Refer to the Appendix for definitions of vectors. The error in each distance was determined using the corresponding known distance from the manufacturing plans. The pooled standard deviation of the error in the distances was computed from the 24 error values (six distances/specimen $\times$ four specimens). This value served as the target for the first application of the Monte Carlo technique.

In the first application of the Monte Carlo technique, a random, independent, and normally distributed error value with zero mean and specified variance was added to each x, y, and z coordinate of the center of each sphere (e.g., $\mathbf{r}_g^{p1/g0} + \mathbf{e}_g$, where $e_x \neq e_y \neq e_z$) measured for one of the specimens (one specimen was used here because each specimen had a unique global coordinate system, which ruled out the use of the average measured coordinates for each sphere). The six distances between each pair of Delrin spheres were then computed, and the standard deviation of the error in the distances was determined. The standard deviation of the distances was computed enough times to find a pooled standard deviation (hereafter termed computed coordinate precision) stable to two decimal places. The variance of the random, normally distributed error applied was iteratively changed until the computed standard deviation of the distances equaled the target value.

The variance found in the first application of the Monte Carlo technique was used to define the random, independent, and normally distributed error with zero mean applied to each coordinate input ($\mathbf{r}_g^{p1/g0}, \mathbf{r}_g^{p2/g0}, \mathbf{r}_g^{p3/g0}, \mathbf{r}_g^{p4/g0}, \mathbf{r}_g^{p5/g0}, \mathbf{r}_g^{p6/g0}, \mathbf{r}_g^{p7/g0}, \mathbf{r}_g^{p8/g0}$) in the adjustment algorithm in the Appendix. The pooled standard deviations of the adjustment values (A-P and M-L translations (Eqs. (A26) and (A27)) for translational standard deviations and F-E and V-V rotations (Eqs. (A33) and (A34)) for rotational standard deviations) were computed until the pooled standard deviations (hereafter termed adjustment precisions) were stable to two decimal places.

Results

Alignment was successful for all four knees. The vectors describing the mechanical axis of the tibia and the loading axis of the apparatus after application of the computed adjustment values were collinear for all four specimens (Fig. 4). Further, the computed adjustment values were relatively small (Table 1), indicating a good initial approximation of alignment during potting of the tibia.

The precision inherent to the MR imaging in determining distances between pairs of spheres in the 4-DOF device was 0.56 mm. From the first application of the Monte Carlo technique, the coordinate precision that corresponded to this error was

Table 1 Values required to adjust the 4-DOF attachment device in each degree of freedom for each of four cadaveric knees

Specimen	A-P (mm)	M-L (mm)	V-V (deg)	F-E (deg)
1	−4	1	−0.5	1.0
2	−2	3	0.5	1.5
3	−12	1	−1.0	1.0
4	7	2	−1.0	1.5

0.40 mm. From the second application of the Monte Carlo technique, the precisions in the translational and rotational adjustments were 1.20 mm and 0.90 deg, respectively.

Discussion

Given the need to achieve specified loading in knee compression studies, the objectives were (1) to develop a MRI-based alignment method for use with apparatuses applying tibiofemoral joint compression, (2) to demonstrate the usefulness of the method by aligning cadaveric knees in an apparatus that could apply tibiofemoral joint compression, and (3) to quantify the error associated with the alignment method.

There are several advantages to using our MRI-based alignment method. First, additional equipment required to achieve alignment is minimized. Although an MR scanner is required, using the adjustable 4-DOF device allows alignment in a relatively simple loading apparatus (Fig. 3). This is important because in studies using MRI to investigate the effects of tibiofemoral compression, for example, a simple design is imperative to achieve desired load levels while meeting necessary material, size, and portability constraints such that it can be used in an off-site MR scanner. Determination of functional axes would require that sensors be removable from an MRI-compatible apparatus, which could allow six degrees of freedom of adjustment while minimizing constraining loads at the knee joint [9]. Achieving all of these degrees of freedom would require a complex apparatus that might not meet the portability constraint. Alignment using biplanar radiographs [7] would require additional resources to construct and store an extra alignment jig.

Another advantage is that the amount of time that the specimen is handled using the new alignment method is minimized because adjustment values of the 4-DOF device are determined by computation. This allows the bulk of alignment to be completed prior to insertion of the specimen in the apparatus. The use of bone-holding clamps requires manipulation of the specimen until alignment is achieved [8], and identification of a functional alignment can be arduous and time consuming as a trial and error process [9].

A third advantage is that using MRI in the new alignment method allows noninvasive capture of 3D bony geometry. This is advantageous in that 3D locations are used to systematically define a loading axis, which should result in a more repeatable and reproducible alignment method as compared to operator-dependent alignment using bone-holding clamps.

Additionally, the method could be adapted for use with CT images. Lastly, in studies in which either bone or soft tissue deformation is to be observed using MRI, as might be done for the computation of 3D cartilage deformations [15], establishing an MRI-based loading axis will allow later correlation of the loading axis to observed structural deformations.

While the alignment method described herein focuses on the tibia, the use of a second adjustable device would strengthen the method. The attachment of a similar adjustable device to the end of the femur would allow independent alignment of the femur. This would allow alignment of both bones based on 3D bony landmarks found using MRI, and it would be useful to study tibiofemoral contact in which knees are purposefully misaligned.

The method would also be strengthened by the use of a surface recognition software. In the present study, bony landmarks were located manually by stepping through MR image sets of the distal tibia, device, and knee and by selecting pixel locations of landmarks. The use of an algorithm to determine volumetric models of bones as well as algorithms to define the locations of bony landmarks assumed to be either spheres or points on the surface of the bones might remove operator subjectivity and lead to improved reproducibility between observers. The use of such algorithms might be more efficient for evaluating a larger number of specimens.

Using the Monte Carlo technique was a practical way to quantify the error associated with the alignment method. While specimens could have been reimaged to determine adjustment precisions, the number of imaging sessions required to achieve meaningful data would have been prohibitively expensive and time consuming to perform. The Monte Carlo technique produced average data based on hundreds of simulations of the alignment algorithm and allowed an investigation of the alignment error attributed to inaccuracies in the MR images. The adjustment precisions computed using the Monte Carlo technique (1.20 mm and 0.90 deg) illustrate that an image resolution of 1.48×1.48 mm^2 for images of the Delrin spheres resulted in misalignments comparable to the adjustment resolution of the 4-DOF device (1.0 mm and 0.5 deg).

The use of two 4-DOF adjustable devices manufactured from different materials was not an important source of error in our study. First, the dimensional accuracy in manufacturing the devices was the same; all critical dimensions that affect the alignment were manufactured to within ±0.051 mm. Second, both devices were fabricated and used at room temperature. The maximum length change for a 12.7 mm long Delrin part (the longest dimension of any one part with the largest coefficient of thermal expansion) for a 5 deg maximum expected change in room temperature is 0.043 mm, which is comparable to the manufacturing tolerance. Accordingly, the potential error due to both manufacturing tolerances and material differences of the devices was approximately 20 times less than the 1 mm increment used for translational adjustability. Additionally, during transportation of the device, all parts were locked into position and care was taken not to load the device so that the alignment was affected. Therefore, error due to the use of two adjustable devices was negligible.

Potting the tibia after removing soft tissues was required for rigid fixation of the knee in this alignment method. Initially, whole human cadaveric legs were desired to be used to better simulate the application of the loading method in vivo, and fiberglass casts were placed on the feet of specimens over a plate allowing attachment of the 4-DOF device to the heel. However, the casts did not allow for adequate fixation because specimens inevitably lost fluid to either the air or cast padding, which resulted in loosening of the cast around the foot and ankle. Placing a cast over soft tissues also made it more difficult to initially achieve an approximate visual alignment of the mechanical axis of the tibia with the loading axis as compared to potting the dissected tibia in a clear acrylic tube. This was apparent with the calculation of larger adjustment values for the 4-DOF device attached to casts as compared to those reported in Table 1. Using cast materials may also slow the rate of compressive loading as compared to the stiff fixation achieved by potting the tibia [16], which is undesirable if the tibiofemoral compressive load is to be applied and transmitted quickly, as it occurs during normal walking. The use of cast materials is therefore not recommended for fixing cadaveric specimens in tibiofemoral joint loading studies.

Although an anatomically based compression axis was explicitly defined here, other axis definitions from other knee joint studies could be used [17–19]. The alignment method described in this paper could be adapted to achieve loading along any axis if adjustments from the axis used in this study relative to any other axis were known. True physiological loading could then be

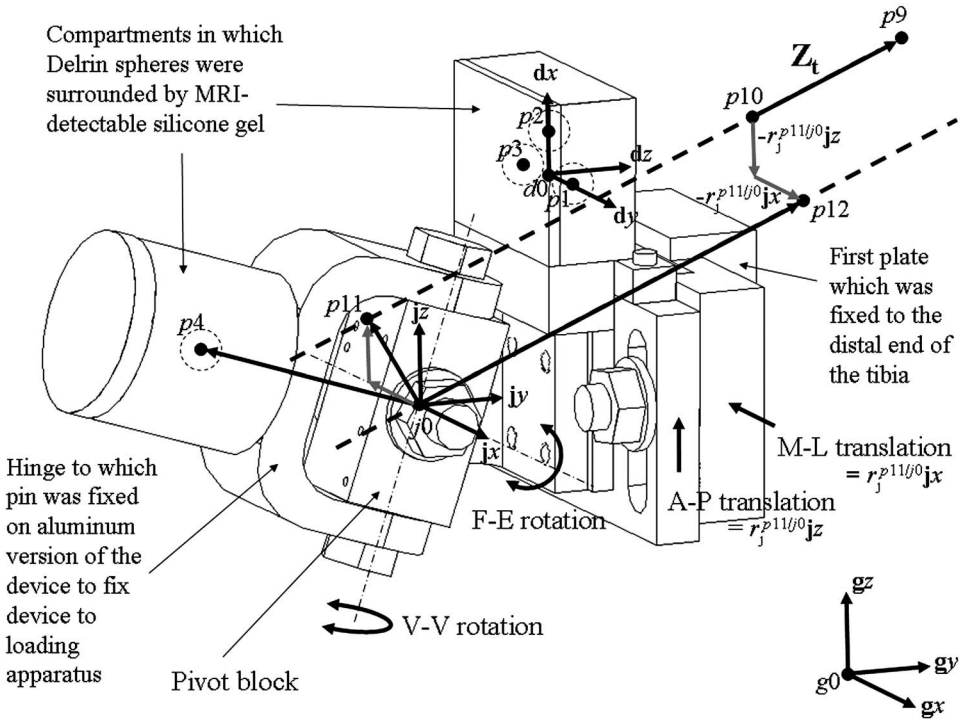

Fig. 5 Diagram illustrating the location of the spatial points and bases used to compute translation and rotation adjustments for the 4-DOF adjustable attachment device. Translation adjustments are also shown here while rotation adjustments are shown in Fig. 6.

achieved for cadaveric studies of tibiofemoral contact. Additionally, a tibiofemoral contact study could be conducted to compare various physiological, mechanical, and functional loading axes.

In summary, this study developed a new MRI-based alignment method for use with apparatuses applying tibiofemoral joint compression. The method was demonstrated by aligning cadaveric knees in an apparatus that could apply tibiofemoral compression, and the errors associated with the alignment method were quantified using the Monte Carlo technique. The alignment method will allow more consistent interpretation of results obtained during tibiofemoral compressive studies conducted using the apparatus described in this paper by providing a well-defined loading axis. The alignment method may also be adapted and/or improved for use with other apparatuses applying tibiofemoral compression.

Acknowledgment

Funding sources including a Floyd and Mary Schwall Fellowship and National Science Foundation Grant No. BES-0096436 are gratefully acknowledged, as are the use of MR scanners and technical assistance gained through the UC Davis Imaging Research Center Pilot Program.

Nomenclature

- n = basis of a Cartesian coordinate system
- $n0$ = origin of a Cartesian coordinate system
- $\mathbf{n}x, \mathbf{n}y, \mathbf{n}z$ = unit vectors for x, y, and z axes of the n basis
- $p1$ = spatial point
- $\mathbf{r}_n^{p1/p0}$ = vector to $p1$ from $p0$ in the n basis
- $r_n^{p1/p0}\mathbf{n}z$ = magnitude of vector to $p1$ from $p0$ in the direction of the unit vector $\mathbf{n}z$ in the n basis
- $[R^{m/n}]$ = matrix of direction cosines to the m basis from the n basis

Appendix

Definition of Landmarks in Magnetic Resonance Images

Bony landmarks and the centers of Delrin spheres were located manually by stepping through collected MR image slices. The lateral and medial eminences were identified in MR images as the center of the eminence in the most proximal image slice in which each eminence could be viewed ($p5$ and $p6$, respectively). Lateral and medial maleoli were assumed to be spheres, and the centers of the maleoli ($p7$ and $p8$) were found in three dimensions by using two-dimensional coordinates of each center identified in two orthogonal planes but taking the average of the redundant coordinate. Similarly, the centers of Delrin spheres were found in three dimensions by using two-dimensional coordinates of each center identified in two orthogonal planes but taking the average of the redundant coordinate.

Calculation of Adjustment Values for the Four Degree-of-Freedom Device

The locations of the centers of the Delrin spheres on the 4-DOF device ($\mathbf{r}_g^{p1/g0}, \mathbf{r}_g^{p2/g0}, \mathbf{r}_g^{p3/g0}, \mathbf{r}_g^{p4/g0}$) and tibial landmarks ($\mathbf{r}_g^{p5/g0}, \mathbf{r}_g^{p6/g0}, \mathbf{r}_g^{p7/g0}, \mathbf{r}_g^{p8/g0}$) defining the orientation of Z_t were first found on the basis of the global coordinate system of the MRI scanner, g (Fig. 5). The center of the tibial eminences and the center of the tibial maleoli were

$$\mathbf{r}_g^{p9/g0} = (\mathbf{r}_g^{p5/g0} + \mathbf{r}_g^{p6/g0})/2 \tag{A1}$$

and

$$\mathbf{r}_g^{p10/g0} = (\mathbf{r}_g^{p7/g0} + \mathbf{r}_g^{p8/g0})/2 \tag{A2}$$

respectively. A local coordinate system d, having an origin $d0$, was defined by the group of three Delrin spheres on the 4-DOF device. The translation to $d0$ from $g0$ on the g basis was determined as

$$\mathbf{r}_g^{d0/g0} = (\mathbf{r}_g^{p1/g0} + \mathbf{r}_g^{p3/g0})/2 \tag{A3}$$

and vectors to the centers of the Delrin spheres on medial and anterior sides of the three-sphere group on the 4-DOF device from $d0$ on the g basis were

$$\mathbf{r}_g^{p1/d0} = \mathbf{r}_g^{p1/g0} - \mathbf{r}_g^{d0/g0} \tag{A4}$$

and

$$\mathbf{r}_g^{p2/d0} = \mathbf{r}_g^{p2/g0} - \mathbf{r}_g^{d0/g0} \tag{A5}$$

Unit vectors were then computed for x, y, and z axes of the d basis by

$$\mathbf{d}_x = d_{xx}\mathbf{g}x + d_{xy}\mathbf{g}y + d_{xz}\mathbf{g}z = \mathbf{r}_g^{p2/d0}/|\mathbf{r}_g^{p2/d0}| \tag{A6}$$

$$\mathbf{d}_y = d_{yx}\mathbf{g}x + d_{yy}\mathbf{g}y + d_{yz}\mathbf{g}z = \mathbf{r}_g^{p1/d0}/|\mathbf{r}_g^{p1/d0}| \tag{A7}$$

and

$$\mathbf{d}_z = d_{zx}\mathbf{g}x + d_{zy}\mathbf{g}y + d_{zz}\mathbf{g}z = \mathbf{d}x\mathbf{d}y \tag{A8}$$

where d_{xx}, d_{xy}, etc. are direction cosines as defined below. The locations of the center of the tibial eminences and center of the tibial maleoli as well as the single Delrin sphere on the distal end of the 4-DOF device were then found on the d basis. First, the matrix of direction cosines to the d basis from the g basis was

$$[\mathbf{R}^{d/g}] = \begin{bmatrix} d_{xx} & d_{xy} & d_{xz} \\ d_{yx} & d_{yy} & d_{yz} \\ d_{zx} & d_{zy} & d_{zz} \end{bmatrix} \tag{A9}$$

Vectors to the center of the tibial eminences, the center of the tibial maleoli, and the center of the single sphere on the end of the device from $d0$ were found on the g basis to be

$$\mathbf{r}_g^{p9/d0} = \mathbf{r}_g^{p9/g0} - \mathbf{r}_g^{d0/g0} \tag{A10}$$

$$\mathbf{r}_g^{p10/d0} = \mathbf{r}_g^{p10/g0} - \mathbf{r}_g^{d0/g0} \tag{A11}$$

and

$$\mathbf{r}_g^{p4/d0} = \mathbf{r}_g^{p4/g0} - \mathbf{r}_g^{d0/g0} \tag{A12}$$

respectively, followed by the determination of these vectors in the d basis by

$$\mathbf{r}_d^{p9/d0} = [\mathbf{R}^{d/g}](\mathbf{r}_g^{p9/d0}) \tag{A13}$$

$$\mathbf{r}_d^{p10/d0} = [\mathbf{R}^{d/g}](\mathbf{r}_g^{p10/d0}) \tag{A14}$$

and

$$\mathbf{r}_d^{p4/d0} = [\mathbf{R}^{d/g}](\mathbf{r}_g^{p4/d0}) \tag{A15}$$

The location of the center of the tibial eminences, the center of the tibial maleoli, and the center of the single sphere on the end of the device were then determined from the center of rotation of the device, $j0$, using the known translation to $j0$ from $d0$ of $\mathbf{r}_d^{j0/d0} = -53.97$ mm $\mathbf{d}x - 41.27$ mm $\mathbf{d}z$ using

$$\mathbf{r}_d^{p9/j0} = \mathbf{r}_d^{p9/d0} - \mathbf{r}_d^{j0/d0} \tag{A16}$$

$$\mathbf{r}_d^{p10/j0} = \mathbf{r}_d^{p10/d0} - \mathbf{r}_d^{j0/d0} \tag{A17}$$

$$\mathbf{r}_d^{p4/j0} = \mathbf{r}_d^{p4/d0} - \mathbf{r}_d^{j0/d0} \tag{A18}$$

These three vectors were then found on the j basis. The matrix of direction cosines to the j basis from the d basis was

$$[\mathbf{R}^{j/d}] = \begin{bmatrix} 0 & 1 & 0 \\ 0 & 0 & 1 \\ 1 & 0 & 0 \end{bmatrix} \tag{A19}$$

and the vectors were computed as

$$\mathbf{r}_j^{p9/j0} = [R^{j/d}]\mathbf{r}_d^{p9/j0} \tag{A20}$$

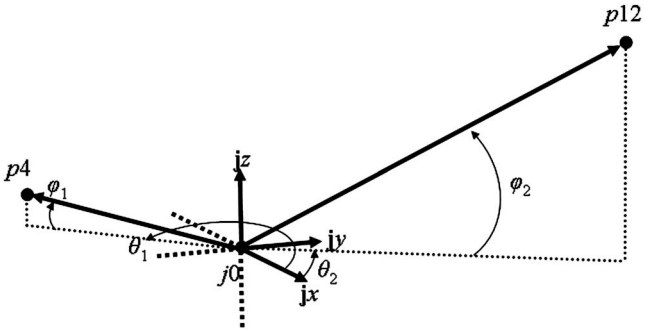

Fig. 6 Angles used to determine V-V and F-E adjustments of 4-DOF devices once A-P and M-L translations were computed

$$\mathbf{r}_j^{p10/j0} = [R^{j/d}]\mathbf{r}_d^{p10/j0} \tag{A21}$$

and

$$\mathbf{r}_j^{p4/j0} = [R^{j/d}]\mathbf{r}_d^{p4/j0} \tag{A22}$$

Once these three vectors were determined on the j basis, the translation adjustments required to align Z_t with the loading axis of the 4-DOF device in these degrees of freedom could be determined. A point $p11$ was defined as being on line Z_t defined by $p9$ and $p10$ (the center of tibial eminences and the center of the tibial maleoli, respectively) and in the $\mathbf{j}x$-$\mathbf{j}z$ plane. As such, the $\mathbf{j}y$ component of the vector to this point from $j0$ was equal to zero ($r_j^{p11/j0}\mathbf{j}y = 0$). The $\mathbf{j}x$ and $\mathbf{j}z$ components of this vector were then found by rearranging equations describing the slope of Z_t (defined by $p9$ and $p10$) and inserting the known $\mathbf{j}y$ component. For three points on a line ($p9$, $p10$, and $p11$ in this particular case),

$$\begin{aligned}(r_j^{p11/j0}\mathbf{j}x - r_j^{p9/j0}\mathbf{j}x)/(r_j^{p10/j0}\mathbf{j}x - r_j^{p9/j0}\mathbf{j}x) \\ = (r_j^{p11/j0}\mathbf{j}y - r_j^{p9/j0}\mathbf{j}y)/(r_j^{p10/j0}\mathbf{j}y - r_j^{p9/j0}\mathbf{j}y) \\ = (r_j^{p11/j0}\mathbf{j}z - r_j^{p9/j0}\mathbf{j}z)/(r_j^{p10/j0}\mathbf{j}z - r_j^{p9/j0}\mathbf{j}z)\end{aligned} \tag{A23}$$

Rearranging these equations and inserting $r_j^{p11/j0}\mathbf{j}y = 0$ resulted in $\mathbf{j}x$ and $\mathbf{j}z$ components of $\mathbf{r}_j^{p11/j0}$ as

$$r_j^{p11/j0}\mathbf{j}x = (0 - r_j^{p9/j0}\mathbf{j}y)(r_j^{p10/j0}\mathbf{j}x - r_j^{p9/j0}\mathbf{j}x)/(r_j^{p10/j0}\mathbf{j}y - r_j^{p9/j0}\mathbf{j}y) + r_j^{p9/j0}\mathbf{j}x \tag{A24}$$

and

$$r_j^{p11/j0}\mathbf{j}z = (0 - r_j^{p9/j0}\mathbf{j}y)(r_j^{p10/j0}\mathbf{j}z - r_j^{p9/j0}\mathbf{j}z)/(r_j^{p10/j0}\mathbf{j}y - r_j^{p9/j0}\mathbf{j}y) + r_j^{p9/j0}\mathbf{j}z \tag{A25}$$

which in turn resulted in A-P and M-L translations required to adjust Z_t such that it intersected $j0$ of the 4-DOF device,

$$\text{A-P translation} = r_j^{p11/j0}\mathbf{j}z \tag{A26}$$

and

$$\text{M-L translation} = r_j^{p11/j0}\mathbf{j}x \tag{A27}$$

V-V and F-E rotations required to complete the alignment of Z_t with the loading axis of the device were then determined. First, point $p12$ was defined as the location of the center of the tibial maleoli on the j basis once A-P and M-L translations were made to the 4-DOF device. This was achieved mathematically by

$$\mathbf{r}_j^{p12/j0} = \mathbf{r}_j^{p10/j0} - \mathbf{r}_j^{p11/j0} \tag{A28}$$

The angles that vectors $\mathbf{r}_j^{p4/j0}$ and $\mathbf{r}_j^{p12/j0}$ made about the $\mathbf{j}z$ axis from the $\mathbf{j}x$ axis (Fig. 6) were determined by

$$\theta_1 = \tan^{-1}(r_j^{p4/j0}\mathbf{j}y / r_j^{p4/j0}\mathbf{j}x) \tag{A29}$$

and

$$\theta_2 = \tan^{-1}(r_j^{p12/j0}\mathbf{j}y / r_j^{p12/j0}\mathbf{j}x) \quad \text{(A30)}$$

and the angles that vectors $\mathbf{r}_j^{p4/j0}$ and $\mathbf{r}_j^{p12/j0}$ made with respect to the $\mathbf{j}x$-$\mathbf{j}y$ plane were determined by

$$\varphi 1 = \sin^{-1}(r_j^{p4/j0}\mathbf{j}z / |\mathbf{r}_j^{p4/j0}|) \quad \text{(A31)}$$

and

$$\varphi 2 = \sin^{-1}(r_j^{p12/j0}\mathbf{j}z / |\mathbf{r}_j^{p12/j0}|) \quad \text{(A32)}$$

The V-V rotation adjustment value was computed as

$$\text{V-V rotation} = (\theta_2 - \theta_1 + \pi)(180 \text{ deg}/\pi) \quad \text{(A33)}$$

and the F-E rotation adjustment value was computed as

$$\text{F-E rotation} = (\varphi 2 - \varphi 1 + \pi)(180 \text{ deg}/\pi) \quad \text{(A34)}$$

References

[1] Paletta, G. A. J., Manning, T., Snell, E., Parker, R., and Bergfeld, J., 1997, "The Effect of Allograft Meniscal Replacement on Intraarticular Contact Area and Pressures in the Human Knee: A Biomechanical Study," Am. J. Sports Med., **25**, pp. 692–698.

[2] Alhalki, M. M., Hull, M. L., and Howell, S. M., 2000, "Contact Mechanics of the Medial Tibial Plateau After Implantation of a Medial Meniscal Allograft: A Human Cadaveric Study," Am. J. Sports Med., **28**, pp. 370–376.

[3] Fukubayashi, T., and Kurosawa, H., 1980, "The Contact Area and Pressure Distribution Pattern of the Knee: A Study of Normal and Osteoarthrotic Knee Joints," Acta Orthop. Scand., **51**, pp. 871–879.

[4] Ihn, J. C., Kim, S. J., and Park, I. H., 1993, "In Vitro Study of Contact Area and Pressure Distribution in the Human Knee After Partial and Total Meniscectomy," Int. Orthop., **17**, pp. 214–218.

[5] Reigger-Krugh, C., Gerhart, T. N., Powers, W. R., and Hayes, W. C., 1998, "Tibiofemoral Contact Pressures in Degenerative Joint Disease," Clin. Orthop. Relat. Res., **348**, pp. 233–245.

[6] Cheng, C. K., Huang, C. H., and Liau, J. J., 2003, "The Influence of Surgical Malalignment on the Contact Pressures of Fixed and Mobile Bearing Knee Prostheses: A Biomechanical Study," Clin. Biomech. (Bristol, Avon), **18**, pp. 231–236.

[7] MacWilliams, B. A., DesJardins, J. D., Wilson, D. R., Romero, J., and Chao, E. Y., 1998, "A Repeatable Alignment Method and Local Coordinate Description for Knee Joint Testing and Kinematic Measurement," J. Biomech., **31**, pp. 947–950.

[8] Dahlkvist, N. J., and Seedhom, B. B., 1990, "Objective Measurement of Knee Laxity and Stiffness With Reference to Knee Injury Diagnosis. Part 1: Design Considerations and Apparatus," Proc. Inst. Mech. Eng., Part H, **204**, pp. 75–82.

[9] Bach, J. M., and Hull, M. L., 1995, "A New Load Application System for In Vitro Study of Ligamentous Injuries to the Human Knee Joint," ASME J. Biomech. Eng., **117**, pp. 373–382.

[10] Pennock, G. R., and Clark, K. J., 1990, "An Anatomy-Based Coordinate System for the Description of the Kinematic Displacements in the Human Knee," J. Biomech., **23**, pp. 1209–1218.

[11] Eckhoff, D. G., Bach, J. M., Spitzer, V. M., Reinig, K. D., Bagur, M. M., Baldini, T. H., and Flannery, N. M. P., 2005, "Three-Dimensional Mechanics, Kinematics, and Morphology of the Knee Viewed in Virtual Reality," J. Bone Jt. Surg., Am. Vol., **87**(Suppl 2), pp. 71–80.

[12] Hollister, A. M., Jatana, S., Singh, A. K., Sullivan, W. W., and Lupichuck, A. G., 1993, "The Axes of Rotation of the Knee," Clin. Orthop. Relat. Res., **290**, pp. 259–268.

[13] Melby, A., III, Noble, J. S., Askew, M. J., Boom, A. A., and Hurst, F. W., 1991, "The Effects of Graft Tensioning on the Laxity and Kinematics of the Anterior Cruciate Ligament Reconstructed Knee," Arthroscopy: J. Relat. Surg., **7**, pp. 257–266.

[14] Grood, E. S., Noyes, F. R., Butler, D. L., and Suntay, W. J., 1981, "Ligamentous and Capsular Restraints Preventing Straight Medial and Lateral Laxity in Intact Human Cadaver Knees," J. Bone Jt. Surg., Am. Vol., **63**, pp. 1257–1269.

[15] Neu, C. P., Hull, M. L., Walton, J. H., and Buonocore, M. H., 2005, "MRI-Based Technique for Determining Nonuniform Deformations Throughout the Volume of Articular Cartilage Explants," Magn. Reson. Med., **53**, pp. 321–328.

[16] Lafortune, M. A., Hennig, E. M., and Lake, M. J., 1996, "Dominant Role of Interface Over Knee Angle for Cushioning Impact Loading and Regulating Initial Leg Stiffness," J. Biomech., **29**, pp. 1523–1529.

[17] Moreland, J. R., Bassett, L. W., and Hanker, G. J., 1987, "Radiographic Analysis of the Axial Alignment of the Lower Extremity," J. Bone Jt. Surg., Am. Vol., **69-A**, pp. 745–749.

[18] Van Sint Jan, S., Hilal, I., Salvia, P., Sholukha, V., Poulet, P., Kirokoya, I., and Rooze, M., 2003, "Data Representation for Joint Kinematics Simulation of the Lower Limb Within an Educational Context," Med. Eng. Phys., **25**, pp. 213–220.

[19] Grood, E. S., and Suntay, W. J., 1983, "A Joint Coordinate System for the Clinical Description of Three-Dimensional Motions: Application to the Knee," ASME J. Biomech. Eng., **105**, pp. 136–144.